

Design and Analysis of Mach-Zehnder Interferometer PICs

Ella Yan

Department of Engineering Physics
University of British Columbia

Abstract—This project focused on the design, simulation, and experimental analysis of Mach-Zehnder Interferometer (MZI) photonic integrated circuits (PICs). Two chips were designed: Chip 1, fabricated by Applied Nanotools using electron beam lithography, and Chip 2, fabricated at the University of British Columbia (UBC) with integrated distributed feedback (DFB) lasers using the Shuksan photonic wire bonding process. Chip 1 targeted free spectral ranges (FSRs) of 23–26 GHz and was designed to enable repeated measurements across multiple MZIs. Chip 2 aimed to characterize MZI behavior with an integrated on-chip laser source. Compact modeling using Python and Ansys Lumerical was performed to predict device performance, and experimental measurements were compared to simulations. Chip 1 results showed good agreement with predictions, while Chip 2 exhibited higher-than-expected FSRs and noisy data, likely due to fabrication defects and coupling losses.

Index Terms—Mach-Zehnder interferometer, Silicon Photonics, Photonic Integrated Circuits, Photonic Wire Bonding

I. INTRODUCTION

Mach-Zehnder Interferometers (MZIs) are widely used in photonic circuits due to their ability to convert phase differences into intensity modulation, making them essential for applications such as optical communication and signal processing. In this project, two chips were designed and modeled: Chip 1 was designed to be fabricated by Applied Nanotools using electron beam lithography, and Chip 2 was designed to be fabricated at UBC, using the Shuksan photonic wire bonding process to integrate a DFB laser onto the photonic chip. The aim was to develop compact models to predict device behavior and to gain experience with both designing and analyzing an MZI. For Chip 1, the goal was to fit multiple MZIs with varying free spectral ranges (FSRs) around 25GHz onto a single chip to allow for repeated measurements and characterization across different designs. The MZIs were designed for operation in the O-band around 1310nm, a key wavelength range for optical communication. For Chip 2, the focus was on analyzing how the MZI behaved when integrated with an on-chip DFB laser.

II. THEORY

A. Mach-Zehnder Interferometer

A Mach-Zehnder Interferometer (MZI) splits an optical signal into two paths, introduces a phase difference, and recombines them to produce interference. The resulting output intensity varies with wavelength, forming an interference pattern characterized by the free spectral range (FSR). MZIs

are widely used in optical communications for modulation and filtering applications.

The output intensity can be derived by considering the interference between two optical paths of different lengths.

Assuming:

- L_1 and $L_2 = L_1 + \Delta L$ are the lengths of the two arms,
- $\beta = \frac{2\pi n_{\text{eff}}}{\lambda}$ is the propagation constant,
- α is the propagation loss coefficient,
- E_i is the input electric field,

the electric fields in each arm after propagation are:

$$E_1 = \frac{E_i}{\sqrt{2}} e^{-i\beta L_1 - \frac{\alpha}{2} L_1}, \quad E_2 = \frac{E_i}{\sqrt{2}} e^{-i\beta L_2 - \frac{\alpha}{2} L_2} \quad (1)$$

After recombination at a Y-branch, the output field is:

$$E_o = \frac{1}{\sqrt{2}} (E_1 + E_2) \quad (2)$$

The output intensity is then:

$$I_o = |E_o|^2 = \frac{I_i}{4} \left| e^{-i\beta L_1 - \frac{\alpha}{2} L_1} + e^{-i\beta L_2 - \frac{\alpha}{2} L_2} \right|^2 \quad (3)$$

In the lossless case ($\alpha = 0$), this simplifies to:

$$I_o = \frac{I_i}{2} [1 + \cos(\beta \Delta L)] \quad (4)$$

where $\Delta L = L_2 - L_1$.

B. MZI Transfer Function

The transfer function of the Mach-Zehnder Interferometer (MZI) is modeled based on the interference between two optical paths of different lengths. While the effective index $n_{\text{eff}}(\lambda)$ is often expanded as a Taylor series around a central wavelength λ_0 , in this work a linear approximation was used:

$$n_{\text{eff}}(\lambda) = n_1 + n_2(\lambda) \quad (5)$$

This simplification was justified because the analysis was restricted to a narrow wavelength range, over which n_{eff} exhibited an approximately linear dependence on λ based on simulation results.

The complex propagation constant is given by:

$$\beta_c(\lambda) = \frac{2\pi i n_{\text{eff}}(\lambda)}{\lambda} + \frac{\alpha}{2} \quad (6)$$

where α is the propagation loss coefficient, expressed in Nepers per meter.

The optical fields in the two arms are modeled as:

$$E_1 = \frac{1}{2} \quad \text{and} \quad E_2 = \frac{1}{2} e^{-\beta_c(\lambda)\Delta L} \quad (7)$$

where ΔL is the path-length difference between the two arms.

The resulting output intensity is:

$$I(\lambda) = |E_1 + E_2|^2 \quad (8)$$

Finally, the measured output in dBm is modeled by:

$$\text{Output}(\lambda) = 10 \log_{10}(I(\lambda)) + b \quad (9)$$

where b is an offset parameter.

C. Free Spectral Range (FSR)

The free spectral range (FSR) is the wavelength spacing between consecutive interference maxima and is given by:

$$\text{FSR}_\lambda = \frac{\lambda^2}{n_g \Delta L} \quad (10)$$

The group index n_g describes how the group velocity v_g of an optical pulse relates to the speed of light c :

$$v_g = \frac{c}{n_g} \quad (11)$$

It is defined in terms of the effective index n_{eff} as:

$$n_g = n_{\text{eff}} - \lambda \frac{dn_{\text{eff}}}{d\lambda} \quad (12)$$

where:

- λ is the center wavelength,
- n_g is the group index of the waveguide,
- ΔL is the optical path length difference between the two arms of the MZI.

Here, n_{eff} is the effective refractive index of the guided optical mode and generally varies with wavelength due to material and waveguide dispersion. In contrast, n_g accounts for both the value and slope of $n_{\text{eff}}(\lambda)$ and governs the propagation of optical pulses through the waveguide.

Finally, the FSR can also be expressed in terms of frequency spacing $\Delta\nu$:

$$\Delta\nu \approx \frac{c}{n_g \Delta L} \quad (13)$$

where c is the speed of light in vacuum. where:

- λ is the center wavelength,
- n_g is the group index of the waveguide.
- c is the speed of light in vacuum ($c \approx 3 \times 10^8$ m/s).

D. DFB Laser Theory and Rate Equations

The behavior of a Distributed Feedback (DFB) laser can be modeled using two coupled rate equations: one for the carrier density (N) and one for the photon density (S). These equations capture the interplay between electrical injection, carrier recombination, stimulated emission, and spontaneous emission.

The system of equations is:

$$\frac{dS}{dt} = \left(G - \frac{1}{\tau_p} \right) S + R_{\text{sp}} \quad (14)$$

$$\frac{dN}{dt} = \frac{\eta I}{q} - \frac{N}{\tau_s} - GS \quad (15)$$

where:

- S is the photon number inside the cavity,
- N is the carrier number,
- G is the material gain,
- τ_p is the photon lifetime,
- τ_s is the carrier lifetime,
- R_{sp} is the spontaneous emission rate,
- η is the injection efficiency,
- I is the injected current,
- q is the elementary charge (1.6×10^{-19} C).

The material gain G is modeled linearly as:

$$G = G_0(N - N_{\text{tr}}) \quad (16)$$

where:

- G_0 is the differential gain coefficient,
- N_{tr} is the transparency carrier density.

The threshold carrier density, transparency carrier density, and material gain coefficient can be calculated using the following relations:

$$N_{\text{th}} = \frac{I_{\text{th}} \eta_i \tau_s}{qV} \quad (17)$$

where:

- I_{th} is the threshold current,
- η_i is the injection efficiency,
- τ_s is the carrier lifetime,
- q is the elementary charge,
- V is the active volume.

The transparency carrier density is then:

$$N_{\text{tr}} = \gamma N_{\text{th}} \quad (18)$$

where γ is the transparency factor.

The differential gain coefficient k is given by:

$$k = \frac{1}{\tau_p(N_{\text{th}} - N_{\text{tr}})} \quad (19)$$

where τ_p is the photon lifetime.

These equations can be numerically integrated to simulate response of the laser to different injection currents.

III. DESIGN

A. Chip 1

For Chip 1, the objective was to explore how varying the path difference Δ would affect the free spectral range (FSR) of the Mach-Zehnder Interferometer and to see if we could accurately model and design an MZI for target FSRs of 23, 24, 25, and 26 GHz. To improve the reliability of measurements and account for potential fabrication defects, the MZIs were designed to be compact to fit as many as possible on a single chip. The first path length L_1 was set to 16.789 μm , chosen to be as short as possible allow many designs to fit compactly within the chip area. The second path length L_2 was then varied to achieve the desired FSRs, using the relation in Equation 13. The calculation and selection of parameters used in this calculation is detailed in the following section.

Chip 1 housed a total of eight MZIs. From left to right across the chip layout, the targeted FSRs were 23 GHz, 24 GHz, 25 GHz, and 26 GHz, with each FSR design duplicated to enable repeated measurements. The MZIs were also given a label with the left most MZI being MZI_1 and the rightmost one being MZI_8.

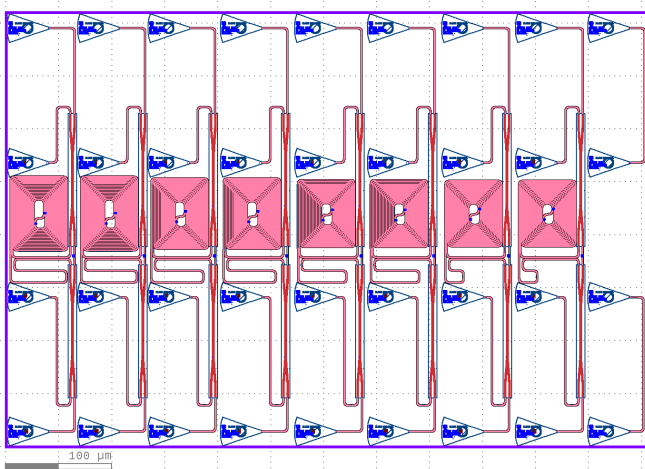


Fig. 1. Layout of Chip 1

Chip 1 was fabricated by Applied Nanotools, who are known to have a process bias of -15 nm and a fabrication variation of ± 10 nm. As such, all design and calculations were done assuming a waveguide core width of 335 nm instead of 350 nm.

B. Chip 2

The goal of Chip 2 was oriented more toward laser integration. A required path length difference was calculated using equation (13) and two arbitrary arm lengths were drawn to satisfy this condition. The only MZI on this chip is located on the bottom left and was designed for a target FSR of 25 GHz.

Chip 2 was manufactured at UBC. The DFB laser was integrated using UBC's Shuksan process. It was assumed that the UBC fab would have a possible process bias of ± 10 nm.

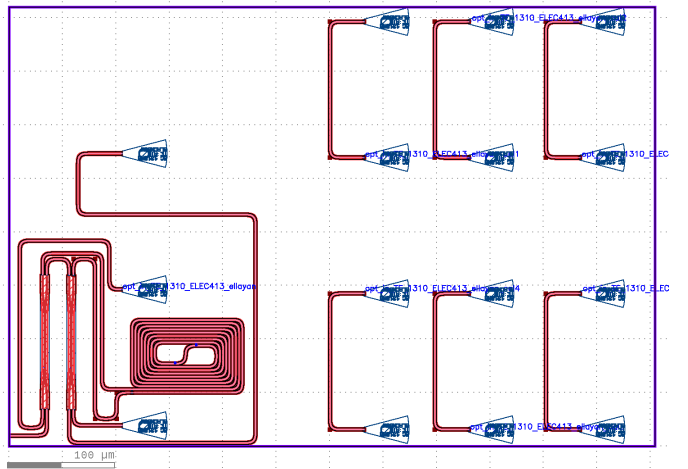


Fig. 2. Layout of Chip 2

IV. MODELING

A. Waveguide Ansys Mode

To obtain the effective and group indices, Ansys MODE was used to simulate the waveguide structures. For Chip 1, the waveguide design consisted of a silicon core with a silicon dioxide cladding. Although the target dimensions were a core width of 350 nm and a height of 220 nm, the manufacturer, Applied Nanotools, is known to introduce a -15 nm fabrication bias. As a result, all simulations were performed assuming a 335 nm core width.

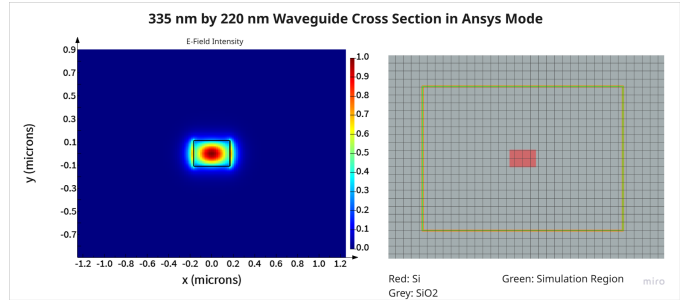


Fig. 3. Ansys MODE Waveguide Simulation For Chip 1

Fabrication variations were considered by varying the waveguide dimensions in the simulations. The path length difference necessary to achieve a 25 GHz FSR was calculated using 13, assuming a perfect 335 x 220nm core waveguide and used as a reference. The effect of changing the waveguide dimensions on the FSR was computed and recorded. All simulations were performed at a wavelength of 1310 nm and a temperature of 300 K. (Additional simulations were conducted at varying temperatures but showed no significant change.)

TABLE I
ANSYS MODE WAVEGUIDE SIMULATION RESULTS FOR CHIP 1

Width (nm)	Height (nm)	Group Index	New FSR (GHz)
335	220	4.56158	25
350	220	4.499503	25.344910
340	220	4.531555	25.165642
320	220	4.591867	24.83511
360	210	4.464544	25.543370
350	210	4.486381	25.419040
335	230	4.550814	25.059143

Similar simulations were performed for Chip 2, which features a silicon waveguide measuring 350nm in width and 220nm in height, with silicon dioxide cladding on the bottom and air cladding on all other sides.

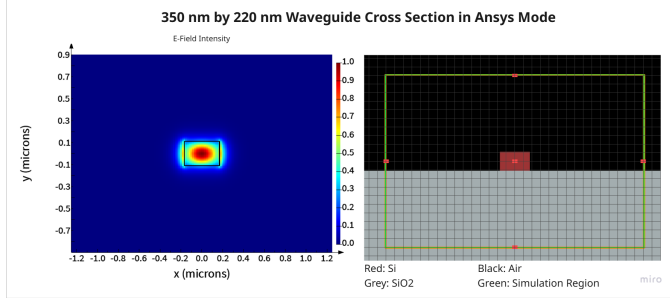


Fig. 4. Ansys MODE Waveguide Simulation For Chip 2

Since this chip was fabricated at UBC, the -15 nm fabrication bias observed in Chip 1 was no longer considered though general fabrication bias was still taken into account. Ansys MODE was used to simulate the waveguide and extract the group index, accounting for potential fabrication variations. A path length difference was calculated assuming a perfect 350 x 220nm core waveguide and used as a reference. The effect of changing the waveguide dimensions on the FSR was computed and recorded.

TABLE II
ANSYS MODE WAVEGUIDE SIMULATION RESULTS FOR CHIP 2

Width (nm)	Height (nm)	Group Index	New FSR (GHz)
350	220	4.785922	25
340	220	4.853419	24.65232241
360	220	4.721834	25.33931731
360	210	4.734105	25.27363673
340	230	4.840704	24.71707628

All simulations were done using a finite difference eigen-mode solver with approximately 150-300 mesh cells in each direction. The refractive index data for Silicon and silicon dioxide were taken from the Palik material database.

It was determined that the fabrication variation could have a noticeable, effect on the FSR, but would likely only cause the FSR to deviate by 0.2-0.3 GHz which was deemed acceptable enough to move on with the experiment.

Effective index as a function of wavelength was found by performing a frequency sweep in Ansys MODE and performing a linear fit.

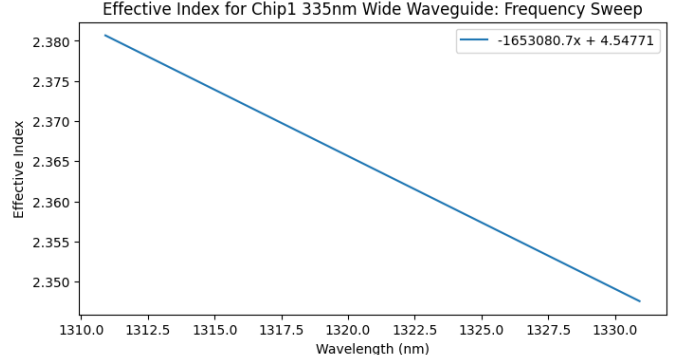


Fig. 5. Effective Index for Chip 1 Frequency Sweep

The process was repeated for both Chip 1 and Chip 2.

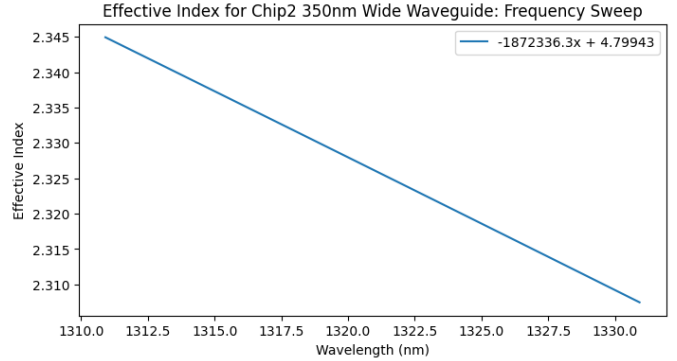


Fig. 6. Effective Index for Chip 2 Frequency Sweep

B. MZI Python Model Chip 1

The FSR equation (13) was used to determine the optical path length differences required to achieve target FSR's of 23, 24, 25, and 26 GHz. The reference arm length L_1 was set to 16.789 μm to satisfy physical size constraints during chip fabrication. The second arm length L_2 was adjusted accordingly to achieve the desired ΔL for each case. Calculations were done assuming a waveguide width of 335 nm.

TABLE III
PATH LENGTHS FOR CHIP 1 FOR VARYING TARGET FSRs

FSR (GHz)	L1 (um)	L2 (um)	ΔL (um)
23	16.789	2874.23197	2857.44297
24	16.789	2755.17185	2738.38285
25	16.789	2645.63653	2628.84753
26	16.789	2544.52701	2527.73801

Similar calculations were done for chip 2 to target a 25 GHz FSR. chip 2 L_1 was set to be 43.851 μm . The required path length difference ΔL , was calculated to be 2505.619 μm .

This resulted in L_2 equaling 2549.470 μm .

After finding the path lengths, the MZI designs were simulated in Python using the equations mentioned in section II.A. It's worth noting that our chip designs use 50/50 directional couplers rather than Y-splitters and combiners, hence the two ports. An example of one of the MZI spectra is plotted below.

TABLE IV
INPUT PARAMETERS FOR MZI SIMULATION

Parameter	Value
Target FSRs (GHz)	23, 24, 25, 26
$\Delta L(\mu\text{m})$	2857.442, 2738.384, 2628.848, 2527.738
$L_1(\mu\text{m})$	16.789
Group index, n_g	4.56158
Propagation Loss, α (dB/cm)	4
Speed of Light, c (m/s)	3.00×10^8

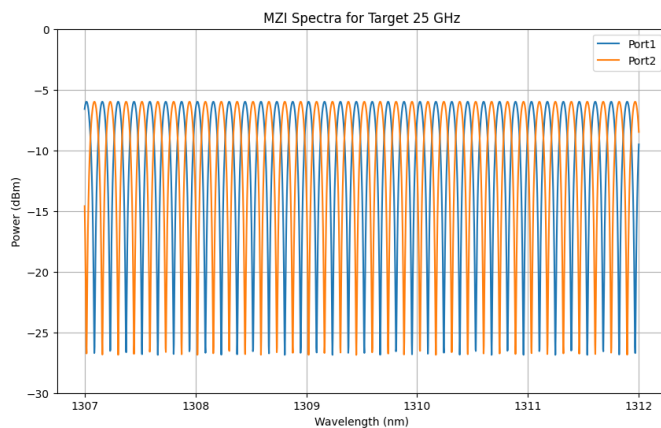


Fig. 7. Simulated MZI Transmission Spectrum for Chip 1 and 25 GHz Target FSR

For each transmission spectrum, the peaks were found using Python and the FSR was calculated. The target FSR vs Python simulation FSR for each design was recorded below.

TABLE V
TARGET FSRs VS FSRS FROM PYTHON SIMULATION FOR CHIP 1 335NM WAVEGUIDE

Target FSR (GHz)	FSR from Simulation (GHz)
23	23.09690
24	24.09175
25	25.09888
26	26.09524

This processes was repeated assuming a waveguide with a 350nm core width to explore the effect that changing the width would have on the FSR.

TABLE VI
TARGET FSRs VS SIMULATED FSRS FOR CHIP 1 350NM WAVEGUIDE

Target FSR (GHz)	FSR from Simulation (GHz)
23	23.33401
24	24.34311
25	25.35495
26	26.37786

C. MZI Interconnect Model Chip 1

Once the circuits were layed out in KLayout, the designs were imported to Ansys Lumerical Interconnect one at a time. Interconnect was used to verify that the designs would produce an oscillator transmission spectrum with an FSR close to the target FSR.

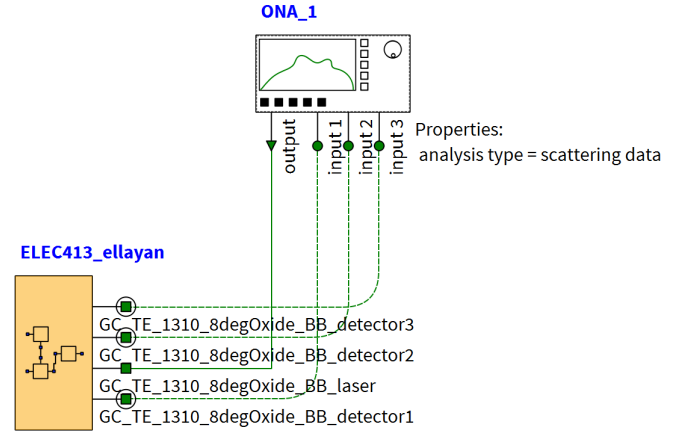


Fig. 8. Interconnect Circuit Ported from KLayout For Chip 1

The resulting transmission spectra were all plotted though only one is displayed here as an example. It was verified that each MZI had the expected oscillatory transmission spectra. Note that only the red and green ports in the image below are output ports. The blue port corresponds to the other input port that is unused.

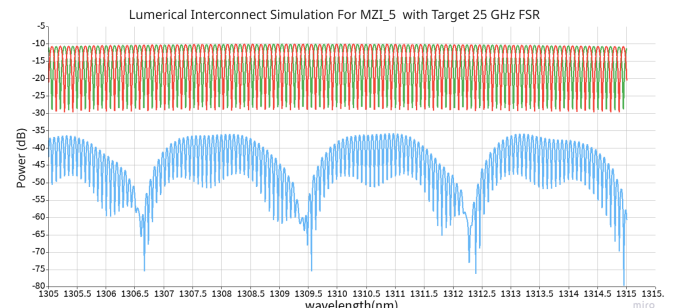


Fig. 9. Example Interconnect Transmission Spectrum For Chip 1

Lumerical Interconnect also calculates the FSR for each transmission spectra. Each MZI on Chip 1 was analyzed in Lumerical Interconnect and their FSRs were recorded in a table.

TABLE VII
TARGET FSRs VS INTERCONNECT FSRs FOR CHIP 1

Label	Target FSR (GHz)	Interconnect FSR (GHz)
MZI_1	23	23.29
MZI_2	23	23.29
MZI_3	24	24.46
MZI_4	24	24.46
MZI_5	25	25.32
MZI_6	25	25.32
MZI_7	26	26.53
MZI_8	26	26.53

It's worth noting that the Interconnect simulation was consistently reporting FSRs that were higher than our expected FSRs using our previous methods. This is likely because the interconnect model components were assuming a waveguide width of 350 nm. It was shown earlier that using the values corresponding to a 350 nm waveguide in the MZI model resulted in higher FSR values from the simulation.

D. MZI and DFB Python Model Chip 2

The MZI modeling aspect for Chip 2, involves the same process and equations as Chip 1, but with slightly different parameter values due to the account for different waveguide.

TABLE VIII
INPUT PARAMETERS FOR MZI SIMULATION FOR CHIP 2

Parameter	Value
Target FSR (GHz)	25
ΔL (μm)	2505.6193
L_1 (μm)	43.851
Group index, n_g	4.7859
Propagation Loss, α (dB/cm)	4
Speed of Light, c (m/s)	3.00×10^8

The resulting spectrum shows the expected oscillatory behaviour.

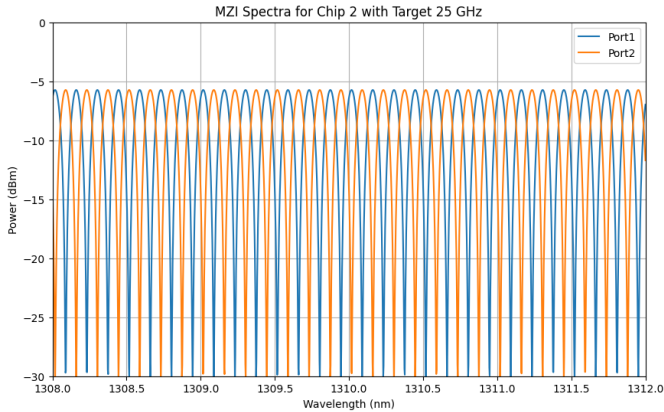


Fig. 10. Simulated MZI Transmission Spectrum for Chip 2 and 25 Ghz Target FSR

The next key component modeled was the Distributed Feedback (DFB) laser. Two approaches were taken: first, a basic model based on datasheet specifications, and second, a

more detailed simulation using laser rate equations.

For the datasheet-based model, the L-I (light-current) curve was generated using the specified threshold current of 13 mA and a slope efficiency of 0.4 mW/mA. A current sweep from 0 to 60 mA was performed to predict the optical output power, resulting in a linear increase beyond threshold, as expected for standard DFB laser behavior.

For the rate equation model, the equations in section II.D were used. SciPy's `odeint` function was used to solve the rate equations. Missing values were approximated and tuned to better match the datasheet model. The parameters used were as follows:

TABLE IX
PARAMETERS USED FOR DFB LASER SIMULATION

Parameter	Description	Value
τ_p (s)	Photon lifetime	3.0×10^{-12}
τ_s (s)	Carrier lifetime	2.0×10^{-9}
G_0 (1/s)	Differential gain	7.0×10^3
N_{tr}	Transparency carrier density	1.5×10^7
η	Injection efficiency	0.4
R_{sp} (1/s)	Spontaneous emission rate	1.0×10^{11}
q (C)	Electron charge	1.6×10^{-19}
h (J·s)	Planck's constant	6.626×10^{-34}
c (m/s)	Speed of light	3.0×10^8
λ_0 (m)	Central wavelength	1270×10^{-9}

From these parameters the following plot was generated.

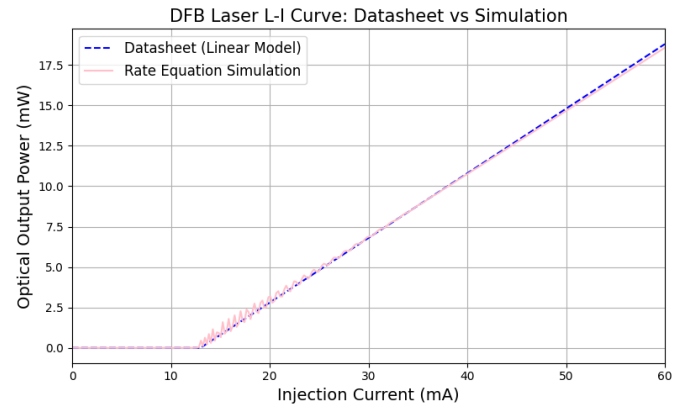


Fig. 11. DFB Laser L-I Curves from Python Simulation

Finally, the DFB laser simulation and MZI simulation were combined. The output power of the DFB laser, as a function of injection current, was used as the input to the MZI model, which computed the optical output power at the corresponding central wavelength. As the laser wavelength shifts with increasing current, the MZI transmission varies periodically, resulting in oscillations in the final optical output power versus current curve.

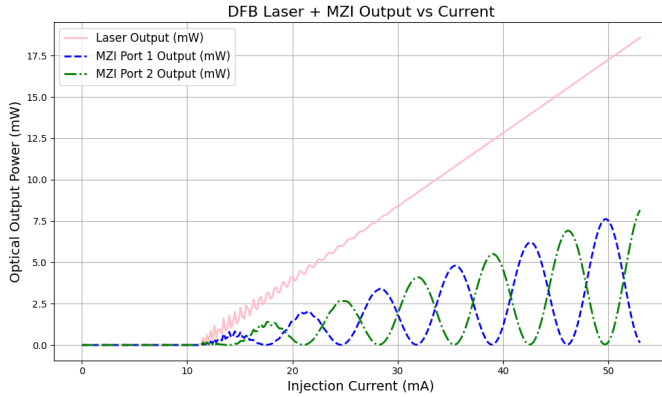


Fig. 12. Simulated DFB Laser Fed into Simulated MZI Chip 2

E. Interconnect Model Chip 2

The chips were designed in KLayout before being ported over to Lumerical Interconnect. They were simulated in the same manner as in Chip 1.

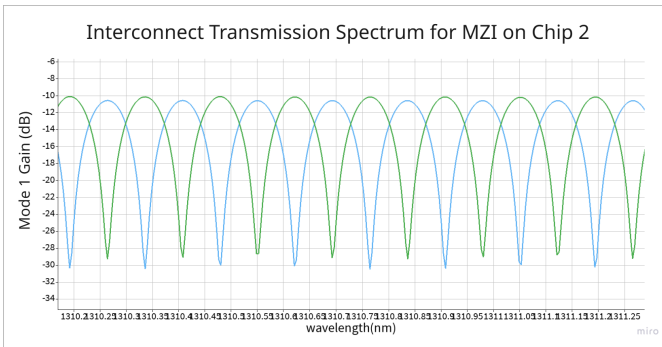


Fig. 13. Interconnect Transmission Spectrum for Chip 2 MZI

The resulting FSR was also plotted in interconnect and was found to be 25.157 GHz which is close to the target 25 GHz. It should be noted that the components used in the interconnect simulation assumed a 350 nm waveguide width, which could explain why the FSR simulated in Interconnect would be larger.

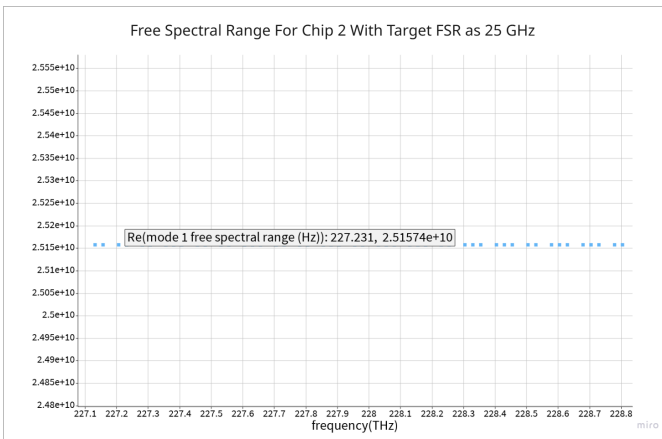


Fig. 14. Interconnect FSR Plot for Chip 2 MZI

V. TESTING

For Chip 1, light was coupled into the photonic devices using grating couplers located at the edges of the chips. A tunable laser source operating in the O-band (1310 nm) was connected to the input grating via an optical fiber, launching light into the on-chip waveguides. For Chip 1, the MZI transmission was measured by connecting output optical fibers to the grating couplers at the ends of each arm, corresponding to Port 1 and Port 2. These output powers were measured using optical power meters or photodetectors connected to an optical spectrum analyzer.

The experimental setup corresponds to a transmission measurement, matching the simulated MZI transfer function that models output power as a function of wavelength. Transmission through each MZI was recorded across a swept wavelength range, allowing extraction of the free spectral range (FSR) and comparison against the predicted spectral behavior from simulations.

For Chip 2, a similar setup was planned, but the optical input was provided by the on-chip DFB laser integrated via photonic wire bonding. Light from the DFB laser was coupled into the photonic circuit through a central grating coupler (Grating Coupler 2). After propagating through the MZI structure, the optical signals were recombined and routed to Grating Couplers 1 and 3. Optical fibers connected to these output grating couplers enabled measurement of the transmitted signals, with GC3 serving as the main signal output and GC1 used to monitor reflections and noise. During on-chip laser measurements, the benchtop tunable laser was turned off. This setup again corresponds to a transmission measurement configuration, allowing comparison between simulated and measured MZI behavior with the integrated laser as the source.

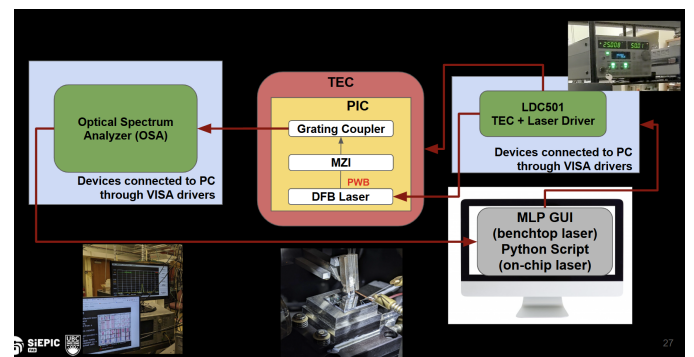


Fig. 15. Testing Block Diagram For Chip 2 [3]

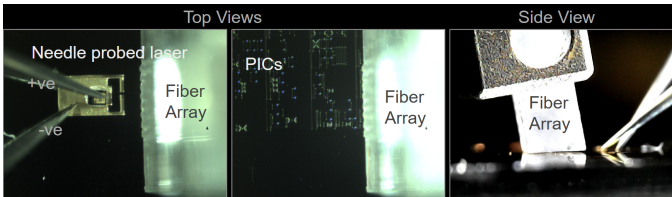


Fig. 16. Testing Set Up For Chip 2

VI. RESULTS AND ANALYSIS

A. Chip 1 Results

Upon initial plotting, all plots looked good except for MZI_8 which appears to just be noise.

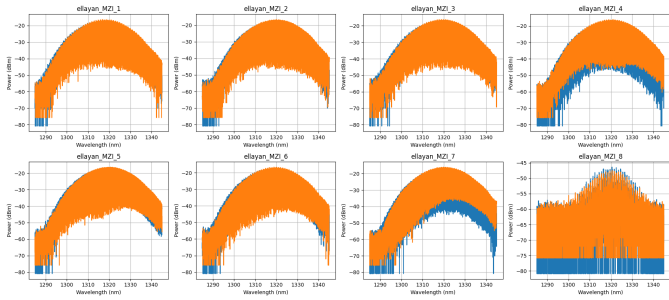


Fig. 17. Transmission Spectra for Chip 1

Zooming in for each plot makes the oscillatory behaviour of the output of the MZI clear.

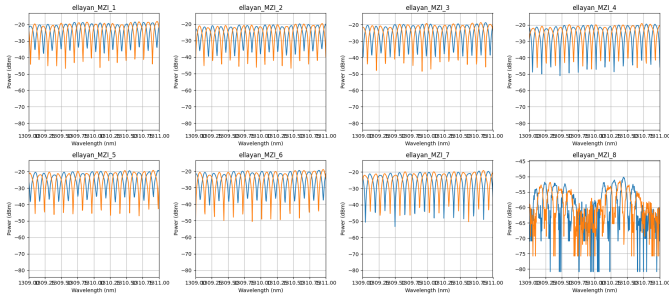


Fig. 18. Transmission Spectra for Chip 1 Zoomed In

There appears to be some oscillatory behaviour in the plot for MZI_8, but the signal is too noisy to properly analyze.

For some preliminary analysis, the peaks in the transmission spectra were found and the differences were measured to calculate the FSR for each MZI and were recorded in the table below.

The data can be visualized on a graph to check for a linear relationship. It appears as though the measured/experimental FSR values are consistently 0/39 GHz higher than expected.

TABLE X
TARGET FSRs VS MEASURED FSRs FOR CHIP 1

Label	Target FSR (GHz)	Measured FSR (GHz)
MZI_1	23	23.37401
MZI_2	23	23.36535
MZI_3	24	24.37794
MZI_4	24	24.40709
MZI_5	25	25.37660
MZI_6	25	25.39412
MZI_7	26	26.43666

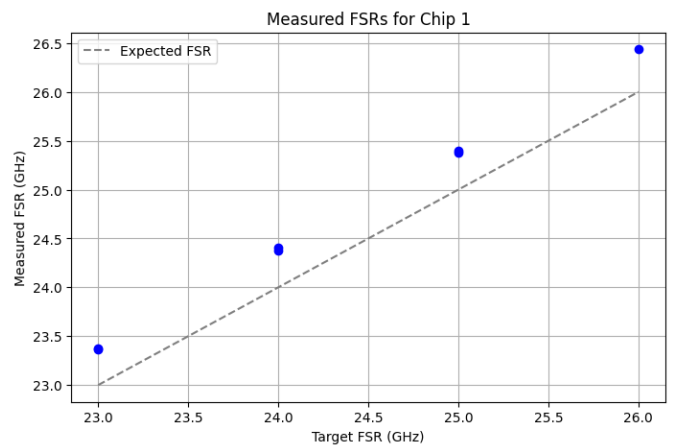


Fig. 19. Baseline Removal For Chip 1

It appears that the repeated designs showed very similar measured FSRs which indicates a not very-impactful process bias. IT is apparent that the measured FSRs are consistently higher than the simulated ones. It could be possible that the manufacturer does not have a -15 nm process or at least not such a strong one, as a wider waveguide resulted in higher FSRs in our sims.

Next the goal was to fit the data to a transfer function to extract more parameters from the data. First step was a baseline removal.

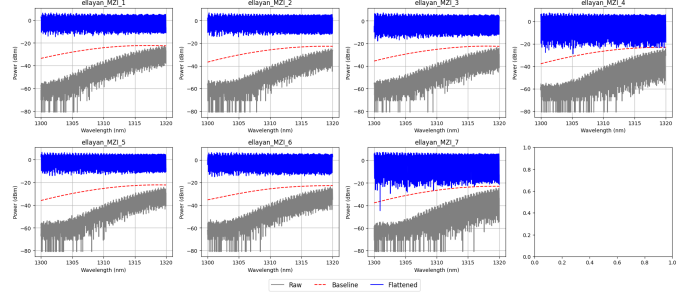


Fig. 20. Baseline Removal For Chip 1

The next step was to fit the MZI transfer mentioned in section II.A.

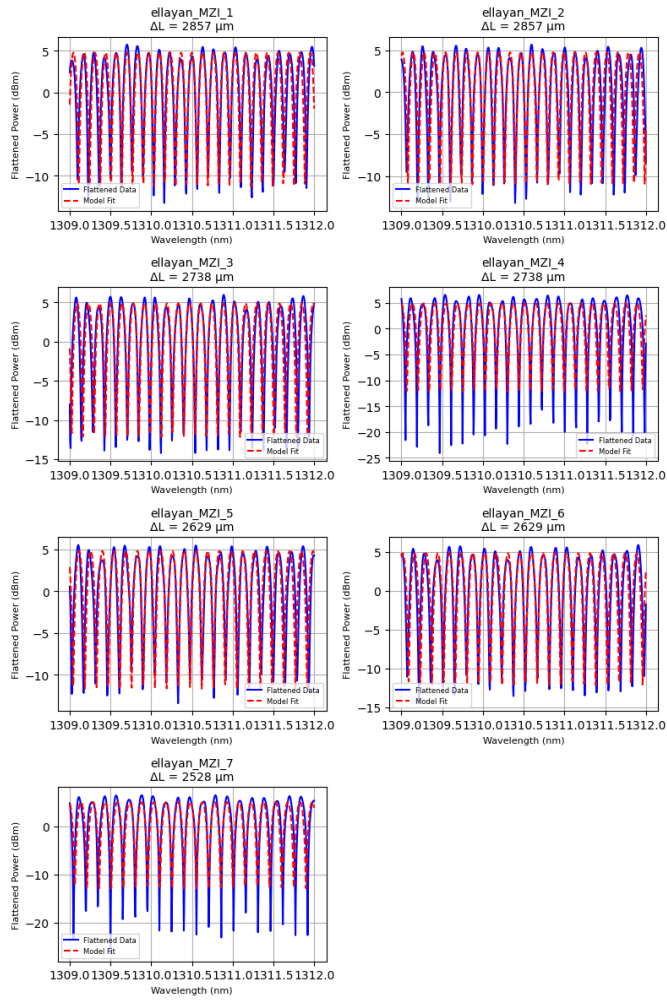


Fig. 21. Transfer Function Fits for Chip 1

Fitting the transfer function allows us to extract some interesting parameters from our data.

TABLE XI
CALCULATED PARAMETERS FROM DATA CHIP 1

Parameter	Mean	Stdev
n_g	4.495	0.0146
n_1	4.548	4.9×10^{-4}
n_2 (1/nm)	-1.653×10^{-3}	2.84×10^{-7}
α	9.3913	0.4779
b	6.0278	0.0266

B. Chip 2 Results

The spectrum for Chip 2 appeared not be as nice as Chip 1. The data was first smoothed for further analysis.

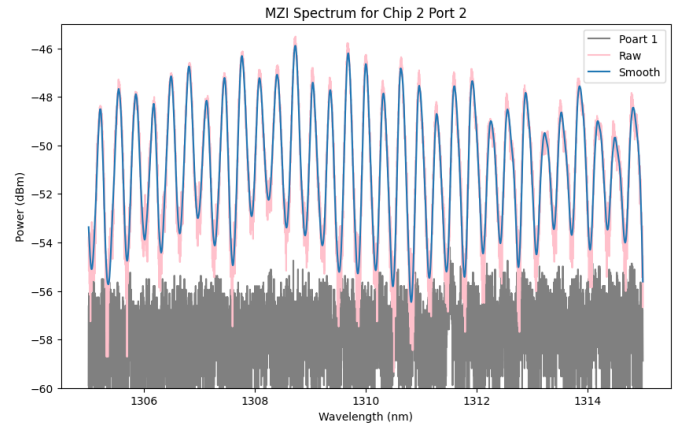


Fig. 22. Raw and Smoothed Transmission Spectra for Chip 2

The location of the peaks were used to calculate the FSR. The FSR calculated was 56.045 GHz. This is not as expected as the target FSR for the design was 25 GHz. The chip was fit to the aforementioned transfer function.

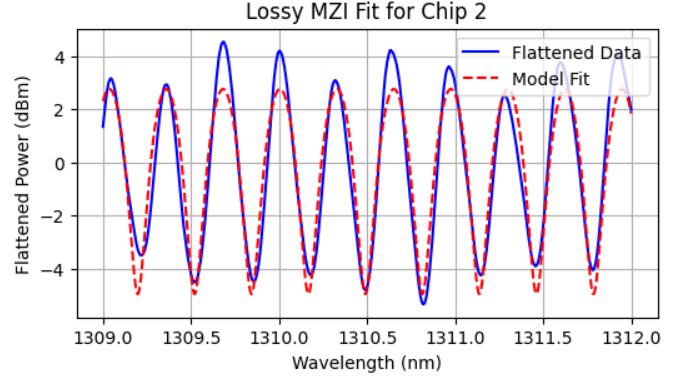


Fig. 23. Transfer Function Fits for Chip 2

TABLE XII
CALCULATED PARAMETERS FROM CHIP 2 DATA

Parameter	Mean
n_1	2.100
n_2 (1/nm)	-1.8727
α	30.0157
b	.7550

The L-I curve for Chip 2 was measured and plotted. The data is noisy but roughly as expected. The optical power remains almost nearly zero until the graph goes past the threshold current (13mA). After that the graph begins to ascend which is as expected. Based on the simulations, some oscillatory behavior should be apparent. It does appear as if the graph goes up, then has a valley, and then continues to go back up but the data is a bit too noisy to be confident that oscillations are apparent. We do see that the optical power

starts rising close to the threshold current and then has an output opposite that of port 1.

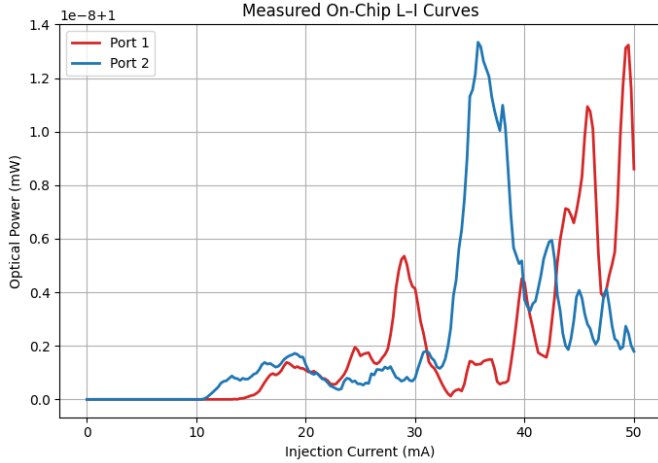


Fig. 24. L-I Curve for Chip 2

VII. DISCUSSION

A. Chip 1 - Larger FSRs

For Chip 1, the Interconnect simulation FSR values and the measured/empirical FSR values were consistently around 0.3-0.4 GHz higher than expected.

It seems likely that assuming a waveguide width of 335nm instead of 350nm was not the correct decision as the path length calculations and simulations when assuming a 350nm wide waveguide produced FSRs that were consistently 0.3 GHz higher than the ones assuming a 335 nm width waveguide.

The Interconnect simulations were autogenerated from the KLayout files and were likely designed around a 350 nm Waveguide. They appear to match more closely to the real FSRs though occasioanlly overshoot by quite a bit. It could be that either the -15 nm fabrication bias wasn't quite right. The one off variations are likely due to general process variations.

B. Chip 2 - Wrong FSR, Noisy Data

The FSR measured for Chip 2 was approximately 56 GHz which is over double the expected FSR. One potential cause could be damage to the chip. There were assembly difficulties with the chips, and some were scratched. Many peers reported having poor quality data for Chip 2 as well, so it may be a process issue rather than a design issue. It would have been good to place at least one other identical MZI on the chip to verify this.

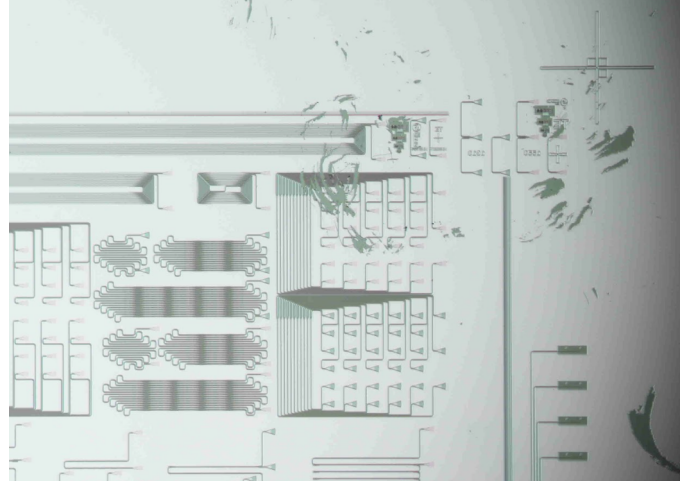


Fig. 25. Chip 2b With Surface Scratches

If these reasons were to be true, they could also explain the noisy data. It could also be due to a poor SNR. The light source for Chip 2 was shared and split among many other chips, which could be why the power output for Chip 2's MZI is generelly lower than the power output for Chip 1's MZI. It's not clear if any design changes could have caused such an decrease in output power.

VIII. CONCLUSION

This project focused on the design, simulation, and experimental characterization of Mach-Zehnder Interferometers (MZIs) on two photonic chips. Chip 1 was successfully designed to explore free spectral range (FSR) variation through controlled changes to the MZI path length difference Experimental results demonstrated general agreement with both our Python simulations as well as our Interconnect Simulations, though measured FSR values were generally higher than originally expected from the Python simulations and regular calculations (equation 13). The most likely cause was the choice to design the MZIs assuming a -15mn shrinkage in width of the waveguide, to account for process bias. Performing simulations assuming no shrinkage tended to produce results that were more similar to the measured results.

Chip 2 aimed to integrate a DFB laser using photonic wire bonding, allowing for on-chip generation of optical signals; however, measurements revealed significant challenges including unexpected FSR values and noisy data. These were likely caused by fabrication defects and coupling losses, as the design process for the MZI was near identical to the process for Chip 1. It would be beneficial in the future to include at least one duplicate of a design on a Chip to rule out fabrication variation or random scratches/accidents. It was difficult to tell if the Python simulations were accurate as the measured data was quite noisy.

Overall, the project provided valuable experience in compact modeling, PIC design, and experimental techniques, while highlighting the importance of accounting for real-world fabrication imperfections in photonic system performance.

ACKNOWLEDGMENT

This project was completed as part of the ELEC 413 course at The University of British Columbia. The devices were fabricated by Applied Nanotools, Inc. using electron beam lithography. Measurements were performed at UBC, with additional support provided by the SiEPIC program. We acknowledge the use of Ansys Lumerical MODE, Python, and KLayout for simulation, modeling, and design.

REFERENCES

- [1] L. Chrostowski and M. Hochberg, "Silicon Photonics Design: From Devices to Systems," Cambridge University Press, 2015.
- [2] L. Chrostowski, "ELEC413 Projects 2025 " SiEPIC FAB, Vancouver, 2025.
- [3] S. J. Chowdhury , "ELEC 413- Laser Integration to PIC Using Photonic Wire Bonding " SiEPIC FAB, Vancouver, 2025.